HHS Public Access

Author manuscript

Nature. Author manuscript; available in PMC 2022 January 28.

Published in final edited form as:

Nature. 2021 December ; 600(7888): 334–338. doi:10.1038/s41586-021-04097-8.

Structural insights into Ubr1 mediated N-degron polyubiquitination

Man Pan[1,5,*], **Qingyun Zheng**[2,5], **Tian Wang**[2,5], **Lujun Liang**[2,5], **Junxiong Mao**[2], **Chong Zuo**[2], **Ruichao Ding**[2], **Huasong Ai**[2], **Yuan Xie**[1], **Dong Si**[4], **Yuanyuan Yu**[1,3,*], **Lei Liu**[2,*], **Minglei Zhao**[1,*]

[1]Department of Biochemistry and Molecular Biology, The University of Chicago; Chicago, IL 60637, USA.

[2]Tsinghua-Peking Center for Life Sciences, Department of Chemistry, Tsinghua University; Beijing 100084, China.

[3]Institute of translational medicine, Shanghai university, Shangda Road 99, Shanghai 200444, China.

[4]Division of Computing and Software Systems, University of Washington Bothell, Bothell, WA 98011

[5]These authors contributed equally to the work.

Abstract

The N-degron pathway targets proteins bearing a destabilizing residue at the N-terminus for proteasome-dependent degradation [1]. In yeast, Ubr1, a single-subunit E3 ligase, is responsible for the Arg/N-degron pathway [2]. How Ubr1 mediates the initiation of ubiquitination and the elongation of the ubiquitin (Ub) chain in a linkage-specific manner through a single E2 ubiquitin-conjugating enzyme (Ubc2) remains unknown. Here, we developed chemical strategies to mimic the reaction intermediates of the first and second Ub transfer steps, and determined the cryo-electron microscopy (cryo-EM) structures of Ubr1 in complex with Ubc2, Ub, and two N-degron peptides, representing the initiation and elongation steps of ubiquitination, respectively. Key structural elements, including a Ubc2 binding region (U2BR) and an acceptor Ub binding loop on Ubr1, were identified and characterized. These structures provide mechanistic insights into the initiation and elongation of ubiquitination catalysed by Ubr1.

[*]Corresponding authors: Minglei Zhao. mlzhao@uchicago.edu; Lei Liu. lliu@mail.tsinghua.edu.cn; Yuanyuan Yu. yuyy@shu.edu.cn; Man Pan. panm@uchicago.edu.

Author contributions

M.P., M.Z., L.L. and Y.Y. designed all the experiments and interpreted the results. M.P., Q.Z. and L. L. designed the synthetic route for chemically synthesized ubiquitination initiation and elongation intermediate mimics. T.W. synthesized the fluorescently labelled Ub-Degron and the elongation intermediate mimic. L.J.L. synthesized the fluorescently labelled Degron and the initiation intermediate mimic. M.P., Y.Y., D.S., and M.Z. performed cryo-EM data collection and processing. J.M. performed the *in vitro* ubiquitination assays with Ubr1 and Ubc2 mutants. Q.Z. performed characterization of the U2BR peptide on the enzymatic properties of Ubc2. T.W., Y.Y., R.D., J.M., H.A. and Y.X. cloned, expressed, and purified Ubr1, Ubc2 and their mutants. M.Z., M.P., and L.L. wrote the paper. M.Z., L.L., Y.Y. and M.P. supervised the project.

Competing interests

The authors declare no competing interests.

Ubiquitination is involved in a wide range of cellular processes [3]. In particular, the N-degron pathway was the first specific pathway of the ubiquitin (Ub) system to be identified [1]. This pathway determines the rate of protein degradation through recognition of the N-terminal residues termed N-degrons. In eukaryotes, N-degrons are recognized by specific ubiquitin ligases (E3) followed by polyubiquitination of a nearby lysine residue, which marks the protein for degradation by the 26S proteasome [4-6]. It was estimated that more than 80% of human proteins could be regulated by the N-degron pathway [7]. Dysregulation of the N-degron pathway leads to proteotoxicity, which underlies ageing and neurodegeneration [8].

In *Saccharomyces cerevisiae* (Baker's yeast), a single E3 ligase, Ubr1, is responsible for the Arg/N-degron pathway, which recognizes two types of N-degrons: type-1 starts with basic residues; type-2 starts with bulky hydrophobic residues [7]. Ubr1 is a single-subunit RING-type E3 ligase with a mass of over 200 kDa (Fig. 1a). Despite being discovered over 30 years [2], the molecular structure of Ubr1 is unknown. More importantly, how Ubr1 catalyses ubiquitination of N-degron remains to be elucidated.

Ubr1 catalyses K48-linked ubiquitination

Previous work has shown that proteins with an Arg/N-degron (43 amino acids) could be polyubiquitinated *in vitro* by yeast Ubr1 and Ubc2 (also known as Rad6) [9]. We synthesized the degron peptide (Degron) and a monoubiquitinated version (Ub-Degron, Extended Data Fig. 1a & b), and reconstituted the polyubiquitination reaction with either peptides as the substrate (Extended Data Fig. 1c-e). When K48R-Ub was used instead of wild-type, the polyubiquitination was substantially reduced (Extended Data Fig. 1e). We performed linkage type analyses using a variant of Degron with a single lysine residue. The results suggested that K48 is the major linkage for the polyubiquitin chain (Extended Data Fig. 2a & b), although a small amount of K63-linked diubiquitin was observed when K48R-Ub was used (Extended Data Fig. 2c). Single-turnover measurement using Degron as the substrate showed a K_m and K_{cat} of 1.24 ± 0.69 μM and 0.27 ± 0.07 min^{-1}, respectively, which represented the initiation step of ubiquitination (Extended Data Fig. 1f). A slightly slower kinetics was observed using Ub-Degron as the substrate, which represented the first step of Ub chain elongation (Extended Data Fig. 1g). Notably, this behaviour was different from that of multi-subunit cullin-RING ubiquitin ligase (CRL), which showed a slow initiation step followed by rapid chain elongation [10,11].

Structure of the initiation complex

A stable complex of Ubc2, Ub and Degron mimicking the reaction intermediate of the initiation step was synthesized (Extended Data Fig. 3a and Supplementary Fig. 1) and mixed with Ubr1, followed by single-particle cryo-EM analyses (Extended Data Fig. 3d, Supplementary Fig. 2a). The final reconstructed map had an overall resolution of 3.35 Å (Extended Data Table 1 and Supplementary Fig. 2b-c). The overall structure of the initiation complex resembled a sailboat (Fig. 1b). The base is a helical scaffold consisting of four regions interspaced by three domains: Ubr-Box1, Ubr-Box2 (also known as the N-domain[12]), and a winged helical domain (WHD) (Fig. 1a, Extended Data Figs. 4a, 5a & b). Similar helical bundle repeats have been observed for other E3 ligases [13-15]. Only

the structure of Ubr-Box1 has been previously reported [16,17]. Ubc2 is primarily bound by a single helix of Ubr1, termed Ubc2 binding region (U2BR, Fig. 1a & b). A RING finger domain follows U2BR and interacts with Ubc2 and the loaded Ub (Extended Data Fig. 5d). A new domain with a novel fold termed cap helical domain (CHD) follows the RING finger domain (Extended Data Fig. 5c). Finally, the UBLC domain (UBR/Leu/Cys domain) [18] interacts with Ubr-Box1 and WHD through a putative zinc-binding site (Fig. 1b & e, Extended Data Fig. 4f). Quadruple mutations of the residues involved in this interface (DHHY mutant) substantially impaired the activity of Ubr1 (Extended Data Fig. 5g).

The first three residues of the Degron were resolved in the conserved pocket of Ubr-Box1 (Fig. 1c, Extended Data Figs. 4d & 6a-b) [16]. The recognition was specific since a Met/N-degron could not be polyubiquitinated (Extended Data Fig. 6c). The active site of Ub transfer is ~35 Å away from the C-terminus of G3, where K17 forms an isopeptide bond with the C-terminal C76 of Ub (Fig. 1d and Extended Data Fig. 4e). The residues between K17 and G3 were not resolved, but the distance indicated an extended conformation (~2.7 Å/residue). Ubr-Box2, homolog of bacterial ClpS [19-21], was resolved in our structure. A superimposition of substrate-bound ClpS suggested that a similar mechanism may be adopted by Ubr1 for type-2 N-degron (Extended Data Fig. 6d-f).

A disulfide bond is formed between C76 of the donor Ub and the catalytic residue of Ubc2 (C88), as designed (Fig. 1d). The donor Ub is on the backside of the complex and interacts with one of the zinc fingers in the RING finger domain through the I36 patch as observed in other E3 complexes [13,14] (Extended Data Fig. 5d). CHD and WHD also participate in the interaction with the donor Ub (Extended Data Fig. 5e). Polyubiquitination was impaired when mutations of these residues were introduced (Extended Data Fig. 5h). In addition to the interactions with the donor Ub, the U2BR of Ubr1 forms an extensive interface with the backside of Ubc2 (Fig. 1b), reminiscent of the Ube2g2 binding region (G2BR) of Gp78 [22], and the Ubc7 binding region (U7BR) of Cue1p [23]. Together, the noncovalent interactions between Ubr1, Ubc2, and Ub position the Ubc2~Ub thioester bond close to the lysine residue of Degron, facilitating Ub transfer.

Structure of the elongation complex

After the first Ub transfer, subsequent chain elongation requires structural rearrangement. Another stable complex mimicking the transition state of the first elongation step was designed and synthesized (Extended Data Fig. 3b-c, Supplementary Fig. 1), followed by single-particle cryo-EM analyses (Supplementary Fig. 3a). The final reconstructed map had an overall resolution of 3.67 Å (Supplementary Fig. 3b-c), with a similar overall structure to that of the initiation complex (Fig. 2a). The linker molecule covalently linked to C88 of Ubc2 forms a disulfide bond with C48 of the acceptor Ub and a peptide bond with G75 of the donor Ub (Fig. 2b and Extended Data Fig. 4g). The F4 patch of the acceptor Ub binds to a loop located in region C of the helical scaffold (termed Ub binding loop, Fig. 2c & Extended Data Fig. 4h), which was disordered in the initiation complex (Fig. 1b). Interestingly, K63 is close to this binding interface. Electrostatic interactions with E880 and D881 may prevent its usage as an acceptor during the elongation reaction (Extended Data Fig. 5f). The acceptor Ub further participated in the recruitment of Ubc2~Ub by binding

at a new interface on Ubc2 (Fig. 2d and Extended Data Fig. 4i). When mutations were introduced into the Ub binding loop of Ubr1 (UBLM mutant) and the new interface (N123 and V124 of Ubc2), the polyubiquitination of Degron and Ub-Degron was substantially reduced (Extended Data Fig. 7a & b). Importantly, UBLM mutant transferred more Ub to Degron than to Ub-Degron (Extended Data Fig. 7a), and single-turnover pulse-chase experiment showed that UBLM mutant failed to transfer fluorescent Ub from Ubc2 to Ub-Degron (Extended Data Fig. 7c), indicating a crucial role of the Ub binding loop in the elongation step.

Compared to the initiation complex, U2BR and Ubc2 (including the donor Ub) underwent a displacement of approximately 18 Å, whereas other domains of Ubr1 remained unchanged (Fig. 2**f**, Extended Data Fig. 7d & e). This displacement of U2BR and Ubc2 repositioned the presumed thioester bond between Ubc2 and the donor Ub so that this bond was approachable by the K48 of the acceptor Ub on Ub-Degron (Fig. 2b). Together, the two complex structures suggested that the displacement of U2BR is the key to accommodating extra Ub during the transition from the initiation to the elongation.

Characterization of E2-E3 interfaces

Both complexes showed an extensive binding interface (823.3 $Å^2$) between U2BR and Ubc2 (Fig. 3a & b). Mutations of interface residues on U2BR (FQFH mutant) and Ubc2 severely impaired polyubiquitination (Extended Data Fig. 7f). The presence of a free U2BR peptide (Ubr1 1165-1200) inhibited polyubiquitination in a dose-dependent manner due to the competitive binding to Ubc2 (Extended Data Fig. 7g). The dissociation constant (*Kd*) was 143 ± 45 nM as measured by isothermal titration calorimetry (Extended Data Fig. 8a). E1-dependent thioester bond (Ubc2~Ub) formation was inhibited in the presence of the U2BR peptide (Extended Data Fig. 8b & c), which was different from G2BR and U7BR [22,23]. The accessibility of the catalytic cysteine (C88) of Ubc2 was decreased in the presence of the U2BR peptide (Extended Data Fig. 7h).

A smaller interface between Ubc2 and the RING finger domain (410.3 $Å^2$ for the initiation complex, 208.2 $Å^2$ for the elongation complex) was observed than in previous studies, such as the interface between UbcH5 and the RING finger domain of TRIM25 (547.4 $Å^2$, Fig. 3c-e) [24], although Ubc2~Ub remained in the closed conformation. Sequence alignment showed that Ubc2 has an asparagine instead of the conserved phenylalanine involved in typical RING-E2 interfaces [25] (Extended Data Fig. 7i). Mutating the asparagine back to phenylalanine decreased ubiquitination activity. Interestingly, the N65A mutation increased the amount of polyubiquitinated Degron (Extended Data Fig. 7j), suggesting that N65 may not be important for the elongation of Ub chain. Indeed, in the elongation complex, a loop around the conserved W96 underwent conformational changes and interacted with the RING finger domain (Fig. 3d, Extended Data Fig. 7i). Due to the flexibility, side-chain density of the loop was not well resolved, but it was clear that the interface is altered in the elongation complex and does not resemble the typical RING-E2 interaction observed in the closed conformation.

Transition from initiation to elongation

The structural changes from the initiation to the elongation complex require Ubc2 to dissociate from Ubr1 so that the newly conjugated donor Ub can move and act as the new acceptor Ub. To test this hypothesis, catalytically inactive Ubc2 (C88S) or non-hydrolysable Ubc2-Ub [26] was pre-mixed with Ubr1 and Degron, followed by ubiquitination assay with wild-type Ubc2. Minimal inhibitory effects were observed, suggesting dissociation of the inactive Ubc2 during the reaction (Extended Data Fig. 8d & e). A complex structure of Ubr1 and Ub-Degron without the presence of Ubc2, named pre-elongation complex, was determined (Supplementary Fig. 4). The map showed greater flexibility with unresolved U2BR. However, the density corresponding to the acceptor ubiquitin on the Ub binding loop was clearly identified (Extended Data Fig. 9a), suggesting that the conjugated ubiquitin could bind at the acceptor Ub site in the absence of Ubc2.

Validation of structural mechanism

We tested several other degron peptides including an Arg/N-degron derived from human protein Rec8 ($^{\text{Hs-Type-1}}$Degron) [27], and a type-2 degron peptide derived from Sindbis virus polymerase nsP4 [28] ($^{\text{Type-2}}$Degron). Wild-type Ubr1 was able to polyubiquitinate both Degron, while mutants of Ubr1 showed decreased activities (Extended Data Fig. 9b & c). Specially, accumulation of monoubiquitinated product in UBLM mutant was observed, confirming the crucial role of Ub binding loop in chain elongation. Furthermore, two truncated native substrates, Scc1 (268-384) [29] and Roq1 (22-104) [30], both containing an N-terminal Arg residue, were tested with similar results (Extended Data Fig. 9d). To validate the structural mechanism in a physiological setting, a previously developed yeast growth assay was performed [29] (Extended Data Fig. 9e). The growth defect of Δ*Ubr1* cells expressing Scc1 was rescued only by co-expressing wild-type Ubr1, not Ubr1 mutants, FQFH and UBLM, suggesting that both U2BR and the Ub-binding loop are critical for Ubr1-dependent N-degron pathway *in vivo* (Extended Data Fig. 9f).

Discussion

Chemical trapping of ubiquitinated intermediates has played critical roles in the mechanistic understanding of various E3 ligases [13,14,31]. Notably, structure of Ubr1 alone showed very flexible CHD and U2BR (Supplementary Fig. 5). After engaging substrates exposing destabilizing N-degrons through the Ubr-Box, and Ub-charged Ubc2 through U2BR and the RING finger domain, Ubr1 facilitates Ub thioester transfer to a Lys residue on the substrate ~40 Å from the very N-terminus (initiation). Ubc2 is released after the first Ub transfer (pre-elongation). The helical scaffold of Ubr1 provides an anchor (the Ub binding loop) for the newly conjugated Ub. After the Ub migrates to the new position, it participates in the recruitment of another charged Ubc2 together with the RING finger domain and U2BR which has shifted to accommodate the acceptor Ub. The interaction between the Ub binding loop and acceptor Ub ensures a close proximity of K48 to the thioester bond of Ubc2~Ub, facilitating the transfer of the second Ub (elongation). We further speculate that similar rearrangements occur for subsequent elongation steps. The most distal acceptor Ub is always

engaged by the Ub binding loop on Ubr1 to ensure linkage specificity of the polyubiquitin chain (Fig. 4).

METHODS

Cloning and plasmid construction

The plasmid containing *Saccharomyces cerevisiae* Ubr1 (pFLAG-UBR1-SBX) was from Addgene (plasmid # 24506) [32]. DNA sequence of yeast (*Saccharomyces cerevisiae*) Ubc2 was synthesized and codon optimized for *E. coli* overexpression by Genscript. The gene was further cloned between the NdeI and XhoI sites of the vector pET-28a containing an N-terminal His tag followed by a HRV3C protease cleavage site. Variants of Ubr1 and Ubc2 were generated using site directed mutagenesis. Human and yeast Uba1 was cloned in pET-28a vector containing an N-terminal His tag. DNA sequences of wild-type ubiquitin (Ub), Ub mutants including K48R, G76C, K0 (all 7 lysine residues mutated to arginine), and AC-Ub (a Ub variant with additional two amino acids Ala-Cys at the N terminus) were synthesized and codon optimized for *E. coli* overexpression by Genscript. The genes were further cloned between the NdeI and XhoI sites of the vector pET-22b. The truncated *Saccharomyces cerevisiae* genes Scc1 (268-384) and Roq1 (22-104) were synthesized by Genscript and cloned into the vector pET-28a containing a His-Sumo tag.

Protein expression and purification

Wild-type Ub and Ub mutants were purified as previously described [33]. Briefly, plasmids for overexpression were transformed to *E. coli* BL21(DE3) competent cells. The *E. coli* cells were grown in Luria broth (LB) media containing 50 μg/mL ampicillin until OD600 reached 0.8 and were induced by isopropyl β-D-1-thiogalactopyranoside (IPTG) at a final concentration of 0.4 mM followed by overnight incubation at 25 °C. Cells were pelleted at 4,000 rpm for 30 min at 4 °C, resuspended in ddH2O and lysed by ultra-sonication for 30 min in an ice bath. The cell lysates were supplemented with 1% perchloric acid to precipitate non-relevant proteins which were then cleared using centrifugation (30 min, 15,000×g, 4 °C). Ub and its variants were further purified using a Mono S cation exchange column (GE Healthcare), followed by dialysis into a buffer containing 50 mM HEPES, pH 7.5, and 150mM NaCl. The peak fractions were pooled and concentrated to 20 mg/ml.

Plasmids containing Ubc2 and its variants were transformed to *E. coli* BL21(DE3) competent cells. The *E. coli* cells were grown in LB media containing 20 μg/mL kanamycin until OD600 reached 0.6, and were induced by IPTG at a final concentration of 0.4 mM followed by overnight incubation at 18 °C. Cells were harvested by centrifugation at 4,000 rpm for 30 min and then lysed by sonication in the lysis buffer (50 mM HEPES, pH 7.5, 150mM NaCl, 20mM imidazole and 1mM PMSF). After centrifugation at 12,000 rpm for 30 min, the supernatant was loaded onto a Ni-NTA affinity column. The proteins were eluted with the elution buffer (50 mM HEPES, pH 7.5, 150mM NaCl, and 400mM imidazole), and further purified by a Superdex 200 size-exclusion column (GE Healthcare) equilibrated in a buffer containing 50 mM HEPES, pH 7.5, and 150 mM NaCl. The expression and purification of Scc1 and Roq1 were similar to Ubc2, except that the Sumo protease Ulp1 was used to cleavage the soluble sumo tag and expose the unstable Arg-terminals.

Yeast Ubr1 and its variants was expressed as previously described [18]. Briefly, single colony of yeast were grown in SD medium at 30°C until OD600 reached ~1.0. The cells were pelleted at 5,000 g, washed once with cold phosphate buffer saline (PBS), and then resuspended (6 mL buffer per 1 g of pellet) in the lysis buffer (50 mM HEPES, pH 7.5, 0.15 M NaCl, protease inhibitor cocktail (Roche), 1mM PMSF, and 10% glycerol,). The resuspended yeast cells were dropped into liquid nitrogen, and the frozen pellet balls were ground to fine powder in liquid nitrogen using a cryogenic impact grinder (SPEX™ SamplePrep 6870 Freezer/Mill). The powder was further thawed and centrifuged at 11,200 g at 4°C for 30 min. The supernatant was loaded onto anti-DYKDDDDK (FLAG) affinity resin (Thermo Scientific, #. A36803), followed by extensive wash. Finally, the FLAG-tagged Ubr1 was eluted with 1mg/mL FLAG peptide and further purified by a Superose 6 size-exclusion column (GE Healthcare) equilibrated in a buffer captaining 50 mM HEPES, pH 7.5, and 150mM NaCl.

Peptide synthesis

All peptides were synthesized using standard Fmoc solid phase peptide synthesis (SPPS) protocols under standard microwave conditions (CEM Liberty Blue). Fmoc-hydrazine 2-chlorotrityl chloride PS resin and Rink Amide MBHA PS resin were used for peptides synthesis. The coupling cycle was programmed as previously reported [34]. Briefly, 10% piperidine in DMF with 0.1 M Oxyma (1 min at 90 °C) was applied as deprotection condition, and 4-fold of 0.2 M Fmoc-protected amino acid, 1.0 M DIC, and 1.0 M Oxyma in DMF (10 min at 50 °C for His and Cys, 90 °C for other residues were applied as amino acid coupling condition. Specifically, in peptide Ub(46-76)-^{K17}Degron-NH_2 and Ub(48-76)-^{K17}Degron-NH_2, Fmoc-Lys (Alloc)-OH was coupled at position 17 for the orthogonal protection. When the backbone coupling was finished, the Alloc protecting group was removed by $[(Ph_3)P]_4Pd/Ph_3SiH$ as previously described [35], and then the ε-amino group on Lys17 can be further coupled with successive sequence (Ub48-76) or (Ub46-76). After the completion of SPPS, the resulting peptide-resin was cleaved in cleavage cocktail (87% trifluoroacetic acid, 5% water, 5% thioanisole, 3% 1,2-ethanedithiol) for 2 h at 25 °C. Crude peptides were precipitated with cold diethyl ether, analyzed and purified by reversed-phase high-performance liquid chromatography (RP-HPLC).

Yeast growth assay

S. cerevisiae strain MAT101 *(MATa lys2-801 ura3-52 trp1-Δ63 his3-Δ200 leu2-3,112)* lacking Ubr1 (*ΔUbr1*) in the BY4741 background was a gift from Dr. Ronggui Hu (University of Chinese Academy of Sciences, Shanghai, China) (Thermo, Cat. no. 95401.H2). The plasmid DHFR–Ub–Arg-Scc1$^{269–566}$ was a gift from Dr. Hai Rao (Southern University of Science and Technology, Shenzhen, China). DHFR–Ub–Met-Scc1$^{269–566}$ was constructed using standard Quick Change PCR, derived from plasmid DHFR–Ub–Arg-Scc1$^{269–566}$. Ubr1 mutants (DHHY, UBLM, FQFH) were constructed in the background of vector Yeplac 181, derived from plasmid #24506 (Addgene) carrying the wild-type Ubr1.

The following *S. cerevisiae* strains were generated: MAT102 (*Ubr1*::*LEU2* in the MAT101 background) and MAT103 (*R-Scc1*::*URA3* in the MAT101 background) expressing full-length Ubr1 and R-Scc1$^{269–566}$ fragment from the P_{GAL-1} promotor; MAT104

(*R-Scc1*::*URA3, Ubr1::LEU2* in the MAT103 background) and a series of derivative strains (MAT105-107) that both express Ubr1 mutants (DHHY, UBLM or FQFH) and R-Scc1$^{269–566}$ fragment from the P_{GAL-1} promotor; MAT108 (*M-Scc1*::*URA3* in the MAT102 background) expressing the wild-type Ubr1 and M-Scc1$^{269–566}$ fragment.

Yeast strains described above were grown in rich (YPD) media containing standard ingredients and 2% glucose. Mid-log phase yeast cultures (2 mL) were gathered by centrifugation and stored in 2 mL fresh YPD medium containing 50% (v/v) glycerol under −80°C for further use. Glycerol stock of different yeast strains (100 μL) was plated onto glucose-containing synthetic-media (SD, -Ura, -Leu) plates and grown for 2 days. Single colony were either plated or spotted in serial 10-fold dilution onto the SD (-Ura, -Leu) and SG (containing 2% galactose rather than glucose, -Ura, -Leu) plates. The plates were incubated for 3 days before pictured.

Preparation of fluorescently labelled Degron and Ub-Degron

Degron was direct obtained from SPPS as described above. K17-linked mono-ubiquitinated degron (Ub-^{K17}Degron) was synthesized from two fragments, Ub(1-45)-$NHNH_2$ and Ub(46-76)-^{K17}Degron-NH_2. Ala46 in the latter fragment was temporally mutated to Cys to enable native chemical ligation of these two fragments. After ligation the thiol group of Cys46 was removed through desulfurization reaction to produce the native Ala46 as shown in Fig S1b. For fluorescence labelling of Degron, we introduced an additional Cys at the C-terminus of Degron to enable site-specific labelling. In the Ub-Degron case, a Cys(Acm) was introduced in the C-terminus of Degron to orthogonally protect this thiol group from being desulfurized. After purification, the Acm group was removed from the Ub-Degron-Cys(Acm) to obtain free thiol group. For labelling reaction, 2 mg lyophilized dry power of Degron-Cys or Ub-Degron-Cys was dissolved in 50 mM HEPES, 150mM NaCl, pH 7.5. Then 2 equivalents of fluorescein-5-maleimide (Invitrogen, #F150) was added and the mixture was incubated at room temperature for 20 min, followed by buffer exchange in (50 mM HEPES, 150mM NaCl, pH 7.5) using a Superdex peptide size-exclusion column (GE Healthcare) to give the fluorescently labelled Degron and Ub-Degron.

Ubiquitination assay with fluorescent Degron or Ub-Degron

In vitro ubiquitination assays were performed with 0.1 μM Uba1, 4 μM Ubc2, 0.25 μM Ubr1, 5 μM fluorescent Degron or Ub-Degron, and 80 μM Ub at 30 °C in the reaction buffer (50 mM HEPES pH 7.5, 0.15 M NaCl, 10 mM $MgCl_2$, and 5 mM ATP). The reactions were terminated by adding 4 × SDS-sample buffer, followed by SDS-PAGE. Unless indicated otherwise, same concentrations of Ubr1 and Ubc2 variants as the respective wild-type were used in the assay.

Single-turnover measurement of Ub transfer in the initiation and elongation steps

To monitor the single-turnover of Ub transfer in the initiation step, i.e., Ubr1 transfers Ubc2~Ub to Degron, a pulse-chase experiment that eliminates the effects of UBA1-dependent formation of Ubc2~Ub intermediate was performed. The pulse reaction generated a thioester-linked Ubc2~Ub intermediate with 5 μM Ubc2, 7.5 μM fluorescent Ub, 0.5 μM UBA1 in a buffer containing 50 mM HEPES pH 8.0, 150 mM NaCl, 2 mM $MgCl_2$,

and 2 mM ATP. The reaction mixture was incubated at room temperature for 10 min, and quenched with 50 mM EDTA on ice for 5 min. A final concentration of 0.5 μM Ubr1 and 25 μM unlabelled Degron was added for the chase reaction which was then incubated at 30°C for 5 minutes. The reaction was stopped by in 2× SDS-sample buffer (pH < 3), followed by SDS-PAGE. Same concentrations of Ubr1 and Ubc2 variants as the respective wild-type were used. The experimental setup for the elongation step was similar to the initiation step, except that fluorescently labelled Ub-Degron was used instead of Degron.

Michaelis-Menten constant (Km) measurement of the initiation and elongation steps

For K_m measurement of the initiation step, two prepared mixtures are required. Mixture 1 consists of Uba1 and Ub (K48R), and Mixture 2 consists of Ubr1 and fluorescently labelled Degron. Both mixtures were prepared in the reaction buffer (50 mM HEPES pH 7.5, 150 mM NaCl, 10 mM $MgCl_2$, and 5 mM ATP). Ubc2 was prepared as a twofold dilution series from the stock, and then introduced into the solution containing equal amounts of the 2 mixtures to initiate the reaction. The final concentrations were 80 μM Ub (K48R), 0.1 μM Uba1, 0.25 μM Ubr1 and 5 μM fluorescently labelled Degron. Reactions were quenched after 1 minute at 30°C using 2 × SDS-sample buffer, followed by SDS-PAGE. The gels were imaged on ChemiDoc MP Imaging System. Substrate and product bands were individually quantified as a percentage of the total signal for each time point using ImageLab (Bio-Rad). Ratios of ubiquitinated products relative to the total signal were plotted against the concentration of Ubc2 and fit to the Michaelis–Menten equation to estimate K_m in GraphPad Prism 8.2.1. The experimental setup for K_m measurement of the elongation step was similar, except that fluorescently labelled Ub-Degron was used instead of Degron.

Generation of the stable complex mimicking the transition state of the initiation step

1. **Preparation of Ub(1-75) hydrazide—**Ub(1-75) hydrazide (Ub75-$NHNH_2$) were generated using previously reported protein hydrazinolysis method [33]. In brief, Ub(G76C) of which Gly76 at the C-terminus was mutated to Cys could undergo N-S acyl transfer so that hydrazine could be used as a suitable nucleophile, leading to a reliable C-terminal hydrazinolysis. 20 mg/mL Ub(G76C), 5 mg/mL TCEP, 50 mg/mL $NHNH_2$•HCl, and 100 mg/mL MesNa were mixed in 20 mM Tris, pH 6.5, and stirred at 60 rpm and 50°C for 24 hours. The final products were purified and analysed by RP-HPLC.

2. **Preparation of Ub(G76C)- ^{K17}Degron—**The reaction scheme was shown in Supplementary Fig. 6a. In brief, Ub75-$NHNH_2$ peptide (1 μmol, 1 equiv) was dissolved in 1mL ligation buffer (6 M guanidinium chloride, 100 mM NaH_2PO_4, pH 2.3) precooled to −15 °C. Then 10 μL 1 M $NaNO_2$ (10 μmol, 10 equiv) was added, and the reaction was stirred for 30 min at −15 °C to fully convert the hydrazide to the acyl azide. Next, sodium 2-mercaptoethanesulfonate (MesNa, 100 μmol, 100 equiv) was added, and the pH was adjusted to 5.0 for overnight reaction. The product, Ub75-MesNa, was further purified by RP-HPLC. Purified Ub1-75-MesNa (1 μmol, 1 equiv) and Cys-^{K17}Degron peptide (1.1 μmol, 1.1 equiv) were mixed to the ligation buffer (6 M guanidinium chloride, 100 mM NaH_2PO_4, 5mg/mL TCEP, pH 7.4). Next, 4-mercaptophenylacetic acid (MPAA, 50 μmol, 50

equiv) was added, and the pH was adjusted to 6.4 for overnight reaction. The final product, Ub(G76C)- ^{K17}Degron, was purified and analyzed by RP-HPLC.

3. Preparation of Ubc2-Ub(G76C)- ^{K17}Degron through disulfide ligation— Lyophilized dry power of Ub(G76C)- ^{K17}Degron (1.3 mg) was dissolved in 100 μL 6 M guanidinium chloride, 50 mM HEPES, pH 7.5 to a final concentration of 1mM. 2 μL of 100 mM 5,5'-dithiobis-(2-nitrobenzoic acid) (Sigma Aldrich, dissolved in 50 mM NaH_2PO_4, pH 7.5) was immediately added and fully mixed by pipetting before incubating at room temperature for 20 min. The solution was then diluted to the refolding buffer containing 50 mM HEPES pH7.5, 150mM NaCl. Excess reactants were removed by a Superdex peptide size-exclusion column (GE Healthcare) equilibrated in the refolding buffer. Finally, the product and 0.9 equiv Ubc2 (pre-dialyzed into the refolding buffer) were mixed and incubated at room temperature for 30 min. The final product was purified and analyzed by RP-HPLC.

Generation of the stable complex mimicking the transition state of the elongation step

1. Preparation of Molecule 2—As shown in Extended Data Fig. 3c, **Molecule 2** was prepared using Cys-aminoethylation reaction[26]. Specifically, 1 μmol lyophilized powder of Ubc2 was incubated in aqueous alkylation buffer (6 M guanidinium chloride, 0.1 M HEPES pH 8.5, 5 mg/mL TCEP) with 40 mM **Molecule 1** (2-((2-chloroethyl)amino)ethane-1-(S-acetaminomethyl)thiol) at 37 °C for 14-16 h. The product, **Molecule 2**, was further purified by semi-preparative HPLC and lyophilized.

2. Preparation of Molecule 3—Lyophilized **Molecule 2** was dissolved in reaction buffer containing 6 M guanidinium chloride, 0.1 M NaH_2PO_4 buffer, pH 7.4 at a final concentration of 1 mM. Then $PdCl_2$ (15 equiv, pre-dissolved in the reaction buffer) was added and the mixture was incubated at 37°C for 1 h to remove the Acm group. Purified Ub(1-75)-MesNa (1 μmol, 1 equiv) and **Molecule 2** (1.1 μmol, 1.1 equiv) were then mixed in the ligation buffer (6 M guanidinium chloride, 100 mM NaH_2PO_4, 5mg/ml TCEP, pH 7.4). Next, 4-mercaptophenylacetic acid (MPAA, 50 μmol, 50 equiv) was added, and the pH was adjusted to 6.4 to initiate native chemical ligation (Extended Data Fig. 3c). The product was purified and analyzed by RP-HPLC.

3. Preparation of Ub^{K48C_K17}Degron—Different from the preparation strategy for Ub-Degron, we mutated the Lys48 to Cys, which enabled native chemical ligation. Furthermore, the thiol group on Cys48 was retained for disulfide ligation. Specifically, Ub(1-47)$NHNH_2$ peptide (1 μmol, 1 equiv) was dissolved in 1mL ligation buffer (6 M guanidinium chloride, 100 mM NaH_2PO_4, pH 2.3) precooled to −15 °C. Then, 10 μL 1 M $NaNO_2$ (10 μmol, 10 equiv) was added, and the reaction was stirred for 30 min at −15 °C to fully convert the hydrazide to acyl azide. Next, Ub(48-76)^{K48C_K17}Degron peptide (1.1 μmol, 1.1 equiv) was added to the ligation buffer, followed by 4-mercaptophenylacetic acid (MPAA, 50 μmol, 50 equiv). The pH was adjusted to 6.4 to initiate the ligation (Supplementary Fig. 6b). The product, Ub^{K48C_K17}Degron, was purified and analyzed by RP-HPLC.

4. Preparation of Ubc2-Ub-Ub^{K48C_K17}Degron using disulfide ligation—

Lyophilized dry power of **Molecular 3** was dissolved in 500ul 6 M guanidinium chloride, 50mM HEPES, 1mM TCEP, pH7.5, and refolded through gradient dialysis against refolding buffer (50mM HEPES, 1mM TCEP, pH7.5) containing 6M, 2M, 1M to 0M guanidinium chloride. 1.3mg Lyophilized dry power of **Ub^{K48C_K17}Degron** was dissolved in 100 μl 6 M guanidinium chloride, 50mM HEPES, pH7.5 (the final concentration was 1mM), and then 2μl 100mM 5,5' -dithiobis-(2-nitrobenzoic acid) (Sigma Aldrich, dissolved in 50 mM NaH_2PO_4 pH 7.5) was added and fully mixed by pipetting before incubating at room temperature for 20 min. The solution was then diluted to the refolding buffer, and the excess small molecular was removed by Superdex peptide size-exclusion column (GE Healthcare) equilibrated in refolding buffer. Finally, the pooled product and 1.1eq refolded **Molecular 3** were mixed and incubated at room temperature for 30 min. The final product, **Ubc2-Ub-Ub^{K48C_K17}Degron**, was purified and analyzed by RP-HPLC.

Specimen preparation for single-particle cryo-EM

Ubr1 (0.4 mg/mL) was mixed with 1.5-fold excess (molar ratio) initiation, or elongation intermediate-mimics and incubated on ice for 30 min. For pre-elongation complex, Ubr1 was mixed with 1.5-fold Ub-Degron on ice for 30 min. A final concentration of 0.01% fluorinated octyl maltoside (FOM) was added to the sample immediately before grid freezing using a Vitrobot mark IV (Thermo Fisher) operating at 8 °C and 100% humidity. A volume of 3.5 μL sample was applied to a glow-discharged Quantifoil Cu 1.2/1.3 grid, and blotted for 1 second using standard Vitrobot filter paper (Ted Pella, 47000-100) before plunge freezing in liquid ethane.

Data collection for single-particle cryo-EM

Optimized frozen grids were sent to Advanced Electron Microscopy Facility at the University of Chicago or National Cryo-Electron Microscopy Facility at National Cancer Institute for data collection. All datasets were acquired as movie stacks with a Titan Krios electron microscope (Thermo Scientific) operating at 300 kV, equipped with a Gatan K3 direct detection camera. A single stack consists of 40 frames with a total exposure around 50 electrons/Å^2. The defocus range was set at −1.0 to −2.5 μm. See Extended Data Table 1 for the details.

Image processing

Movie stacks were subjected to motion correction using MotionCor2 (v1.3.2) [36]. CTF parameters for each micrograph were determined by CTFFIND4 (v4.1.9) [37]. The following particle picking, two- and three-dimensional classifications, and three-dimensional refinement were performed in RELION-3.1 [38]. About 2,000 particles were manually picked to generate 2D class averages. The class averages were then used as templates for the following automatic particle picking. False-positive particles or particles classified in poorly defined classes were discarded after 2D classification. Initial 3D classification was performed on a binned dataset using the initial model obtained in RELION. The detailed data processing flows are shown in Supplementary Figs. 2, 4, 5 and 6. Only small fractions of particles went into the final 3D reconstruction, which may result from several factors.

First, as many particles as reasonable were picked at the beginning to account for rare orientations. Secondly, the efficiency of complex formation may affect the number of useful particles. Finally, other factors such as air water interface and the detergent used to fix the orientation preference may also contribute to the small percentage of particles went into the final 3D reconstruction. Data processing statistics are summarized in Extended Data Table 1. Reported resolutions are based on Fourier shell correlation (FSC) using the FSC=0.143 criterion. Local resolution was determined using the implementation in RELION.

Model building, refinement and validation

Yeast Ubr1 is a single-subunit E3 with 1,950 amino acids. Only the structure of Ubr-Box1 domain was determined previously [16,17]. Artificial intelligence (AI) based de novo modelling tool DeepTracer [39] was used to build a starting model of the entire complex from scratch. Specifically, the sharpened map of the initiation complex and a FASTA file containing sequences of Ubr1, Ubc2, and Ub were input to the online server of DeepTracer (https://deeptracer.uw.edu/home). The program output a complete model with Ubc2, and Ub correctly positioned. About 80% of Ubr1 was correctly built into the cryo-EM map, with some errors in the poorly resolved regions and the zinc-binding sites. The starting model was first refined in real space using PHENIX (v1.15.2) [40], and then manually fixed, adjusted and refined using COOT [41]. About 1800 residues of Ubr1 were built except for some flexible loops and ~140 C-terminal residues. The registration of the main chain was carefully checked and fixed based on bulky residues. The entire procedure was greatly simplified and accelerated with the starting model from DeepTracer. To further improve the geometry of the atomic models, ISOLDE [42] embedded in ChimeraX (v0.9) [43] was used to fix most rotamer and Ramachandran outliers. Multiple rounds of manual model building/optimization in COOT (v0.89) and ISOLDE followed by PHENIX real space refinement were performed. Both sharpened and unsharpened maps were used. The unsharpened maps were used in the earlier iterations. Sharpened maps were used for the final refinement since they have better resolved side-chain density. The resolution of the elongation complex is worse, but some loop areas were better resolved and were used to aid the modelling of the initiation complex. Tetrahedral geometry restraints of the zinc binding sites were applied wherever reasonable. The following strategies have been tried to improve the fitting of the chemical linker in the elongation complex, including changing the expected sigma of customized restraints and applying higher weight on the experimental data during the refinement. Due to the flexibility of the chemical linker, the density around the linker including a loop containing W96 of Ubc2 in the elongation complex was not resolved as well as the rest of the map. Special attention has been paid to model interpretation. The statistics of model refinement and geometry is shown in Extended Data Table 1. Molecular graphics and analyses were performed with UCSF ChimeraX[43] and PISA at the European Bioinformatics Institute (http://www.ebi.ac.uk/pdbe/prot_int/pistart.html) [44]. Structure comparison and domain identification were performed using the DALI server for protein structure comparison [45] and SWISS-MODEL [46].

Ubc2~Ub thioester formation in the presence of U2BR peptide

First, 0.5 μM Uba1, 5 μM Ubc2, and 7.5 μM fluorescently labelled Ub was mixed in the reaction buffer containing 50 mM HEPES pH 8.0, and 150 mM NaCl. U2BR peptide was

prepared as a twofold dilution series from the stock and added to the reaction mixture. Prepared ATP·Mg^{2+} mixture (50 mM $MgCl_2$, 50 mM ATP, pH 8.0) was added to initiate the Ubc2~Ub thioester formation. Reactions were quenched after 10 minute at 30 °C using 2 × SDS-sample buffer (pH < 3), followed by SDS-PAGE. The gels were imaged on ChemiDoc MP Imaging System, and substrate and product bands were quantified respectively as a percentage of the total signal for each time point using ImageLab (Bio-Rad). Ratio of ubiquitylated products relative to the total signal was plotted against the concentrations of Ubc2 and fit to the inhibitor vs. response model (three parameters) in GraphPad Prism 8.

Isothermal titration calorimetry (ITC) analysis

All reported isothermal titration calorimetry data were collected using a MicroCal ITC 200 instrument in the centre of biomedical analysis, Tsinghua University. Ubc2 and all U2BR peptides were buffer exchanged to 50 mM HEPES pH 7.5, and 150 mM NaCl before the experiment. For the experiments, 20 μM Ubc2 solution in the sample cell was titrated with 400 μM U2BR peptide solution through 19 injections (2.0 μL each) at 25 °C and 750 rpm stirring speed. Data fitting and analyses were performed using Origin 7 SR4 (OriginLab).

Extended Data

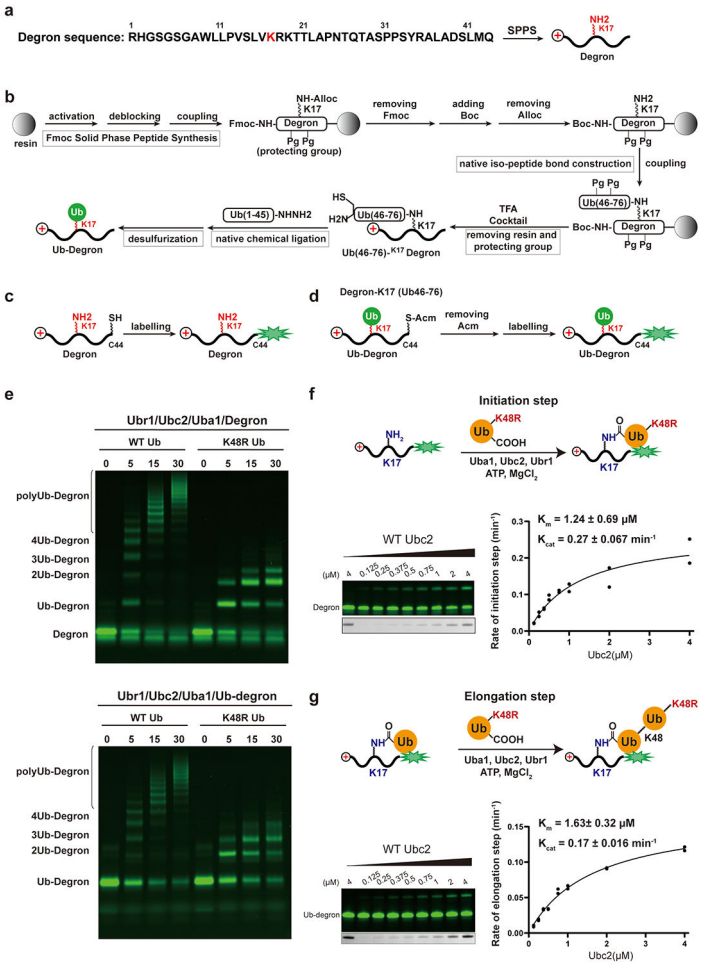

Extended Data Fig. 1: Ubr1-mediated K48-linked polyubiquitination of degron peptides.

a, Amino acid sequence of the degron peptide (Degron). SPPS: solid-phase peptide synthesis. **b**, The synthetic route of the monoubiquitinated degron peptide (Ub-Degron). **c-d**, Fluorescent labelling of Degron (**c**) and Ub-Degron (**d**). An additional C-terminal cysteine was introduced for the labelling of fluorescein-5-maleimide. *e*, *In vitro* Ubr1-dependent ubiquitination assays using fluorescent Degron (top) and Ub-Degron (bottom) as substrates. Gel images are representative of independent biological replicates ($n = 2$). **f-g**, Quantitative evaluation of the kinetics for Ubr1-mediated ubiquitination initiation (**f**) and the first step of elongation (**g**). Averages of two independent experiments were plotted and fit to the Michaelis–Menten model to estimate the K_m and K_{cat}. Gel images are representative of independent biological replicates ($n = 2$).

a

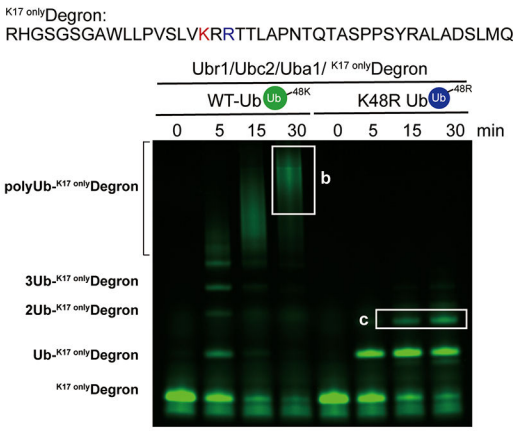

b

MS-MS Result of polyUb-$^{K17\ only}$Degon using WT Ub

Linkage type	Ubiquitin sequence	# PSMs	Modifications	Area
K48	LIFAGkQLEDGR	100	K6(GlyGly)	1.848E11
K48	LIFAGkQLEDGRTLSDYNIQK	14	K6(GlyGly)	4.196E9
K63	TLSDYNIQkESTLHLVLR	17	K9(GlyGly)	1.451E10
K63	TLSDYNIQkESTLHLVLRLR	5	K9(GlyGly)	1.252E9
K11	TLTGkTITLEVEPSDTIENVK	8	K5(GlyGly)	7.329E9
K33	IQDkEGIPPDQQR	4	K4(GlyGly)	2.763E8
K6	mQIFVkTLTGK	1	M1(Oxidation); K6(GlyGly)	1.096E8
K6	MQIFVkTLTGK	1	K6(GlyGly)	7.091E7

c

MS-MS Result of diUb-$^{K17\ only}$Degon using K48R Ub

Linkage type	Ubiquitin sequence	# PSMs	Modifications	Area
K63	TLSDYNIQkESTLHLVLR	13	K9(GlyGly)	2.884E9

Extended Data Fig. 2: Analyses of ubiquitin chain linkage generated by Ubr1.

a, *In vitro* Ubr1-dependent ubiquitination on fluorescently labelled ^{K17only}Degron using wild-type Ub (left) and K48R-Ub (right). Gel images are representative of independent biological replicates (n = 2). Gel slices in box b and c were cut and digested, followed by LC-MS/MS analyses. **b**, Identification of Ub chain linkages in box b. **c**, Identification of Ub chain linkages in box c. # PSMs: Number of peptide spectrum matches.

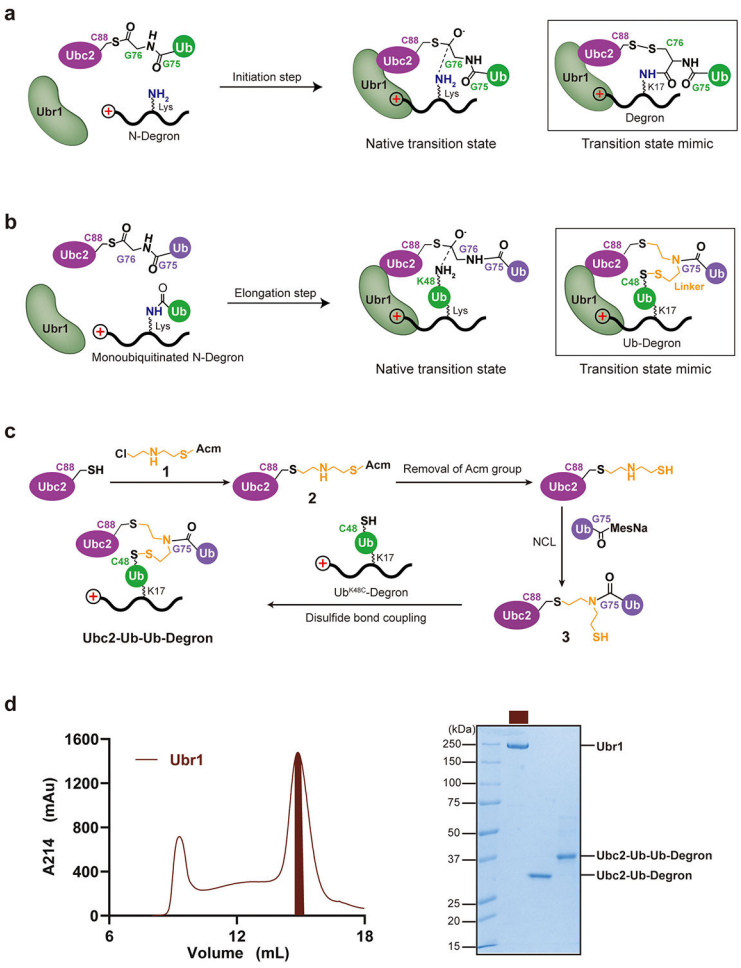

Extended Data Fig. 3: Design and purification of the stable intermediate structures.

a, A schematic representation of the transition state of the initiation step. The side chain of a Lys residue on Degron attacks the thioester bond of Ubc2~Ub. The inset shows the designed intermediate structure mimicking the transition state of the initiation step. **b**, A schematic representation of the transition state of the elongation step. The side chain of K48 on Ub-Degron attacks the thioester bond of Ubc2~Ub. The inset shows the designed intermediate structure mimicking the transition state of the elongation step. **c**, A brief synthetic route of the intermediate structure mimicking the transition state of the elongation step. **d**, A gel filtration chromatogram of Ubr1 (left) and an SDS-PAGE gel of purified Ubr1 and designed stable intermediate structures Ubc2-Ub-Degron and Ubc2-Ub-Ub-Degron (right).

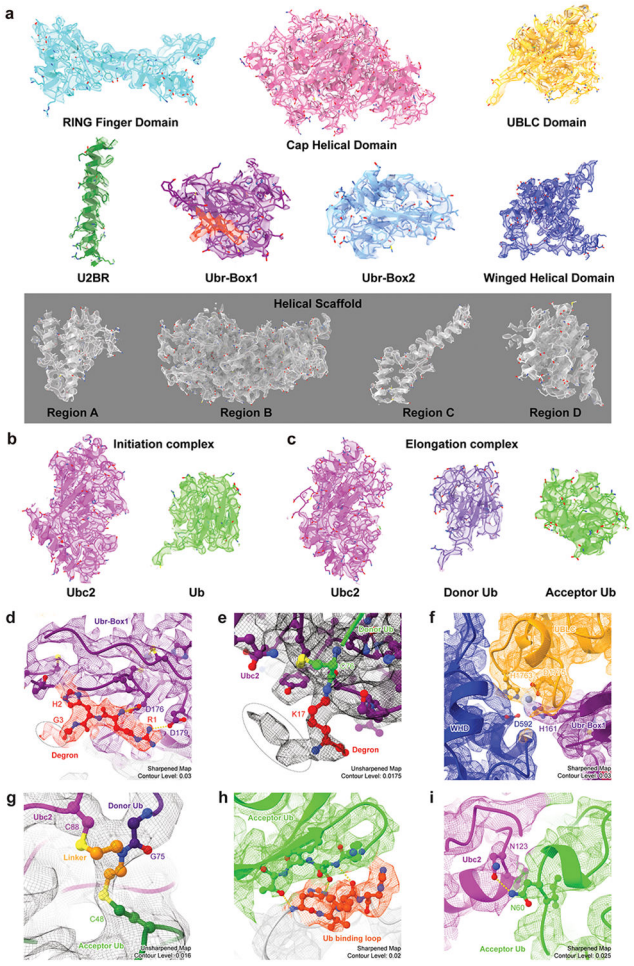

Extended Data Fig. 4: Cryo-EM density of the initiation and elongation complexes.

a, Individual domains of Ubr1 in the initiation complex. **b**, Ubc2 and Ub in the initiation complex. **c**, Ubc2, donor Ub and acceptor Ub in the elongation complex. Maps in panels **a** and **b** were sharpened using a B factor of −96.5 Å^2 and contoured at a level of 0.030. Maps in panel **c** were sharpened using a B factor of −96.7 Å^2 and contoured at a level of 0.022. **d,** Degron recognition site of the initiation complex. **e,** Active site of the initiation complex. **f,** Three-domain junction of the initiation complex. **g,** Active site of the elongation complex. **h,** Acceptor Ub and Ubr1 binding interface in the elongation complex. **i,** Acceptor Ub and Ubc2 binding interface in the elongation complex. Dotted circles in panels **d** and **e** mark the unmodeled densities corresponding to the Degron peptide which are only visible at the low contour levels. Atomic models could not be reliably built into the densities.

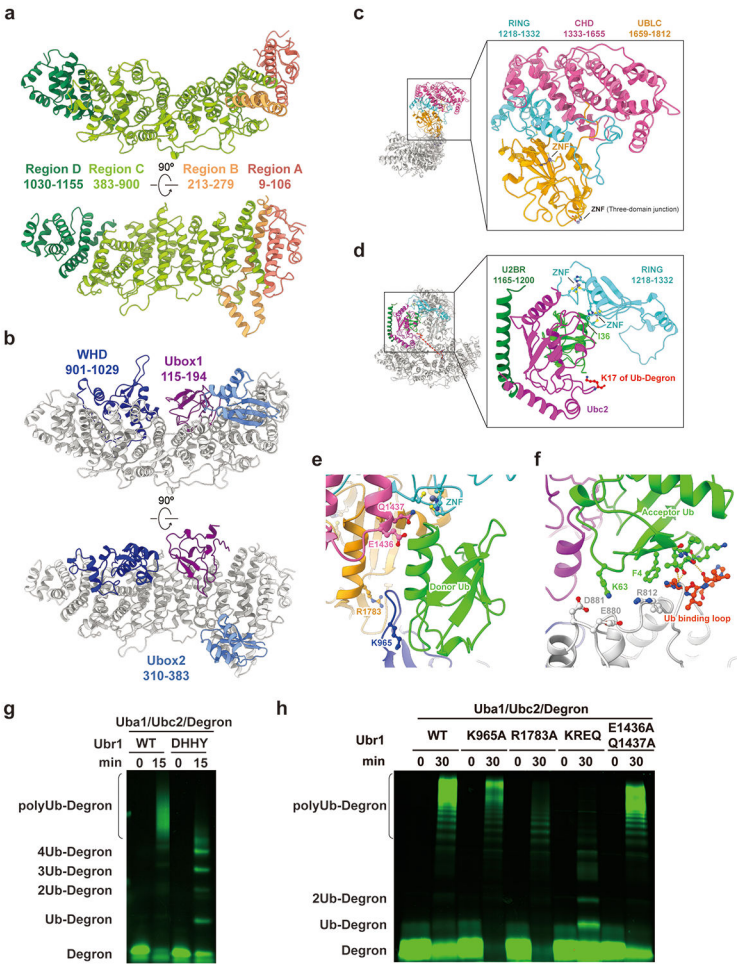

Extended Data Fig. 5: Molecular structures of Ubr1 complex and interfaces between Ubr1 and Ub.

a, The helical scaffold of Ubr1 consists of four separate regions. **b,** The three domains located around the helical scaffold, Ubr-Box1 (Ubox1, purple), Ubr-Box2 (Ubox2, light blue) and winged helical domain (WHD, dark blue). **c,** The three domains above the helical scaffold, the RING finger domain (cyan), cap helical domain (CHD, pink) and UBLC domain (yellow). The RING finger domain is sandwiched between the CHD and UBLC domain. An additional zinc finger motif (ZNF) in UBLC is labelled. **d,** U2BR (forest green), Ubc2 (magenta)~Ub (lime) and the RING finger domain form the catalytic module of Ubr1 complex. Two zinc finger motifs (ZNF) in the RING finger domain are labelled. **e,** Additional binding interfaces between the donor Ub and Ubr1, including K965 in WHD, E1436 and Q1437 in CHD. R1783 in UBLC domain is the key residue to stabilize the loop of WHD. **f,** Additional binding interfaces between the acceptor Ub and Ubr1. **g,** In vitro Ubr1-dependent ubiquitination assay. A quadruple mutant (H161A, Y933A, D1175A, and H1763A, DHHY) of the residues involved in the interface between Ubox1, WHD, and UBLC (three-domain junction, shown in Fig. 1e) was tested. Gel images are representative of independent biological replicates ($n = 2$). **h,** *In vitro* Ubr1-dependent ubiquitination assay. Mutants of Ubr1 including K965A, E1436A/Q1437A, R1783A and K965A/E1436A/

Q1437A/R1783A (KREQ) involved in the interfaces mentioned in panel e were tested. Gel images are representative of independent biological replicates (n = 2).

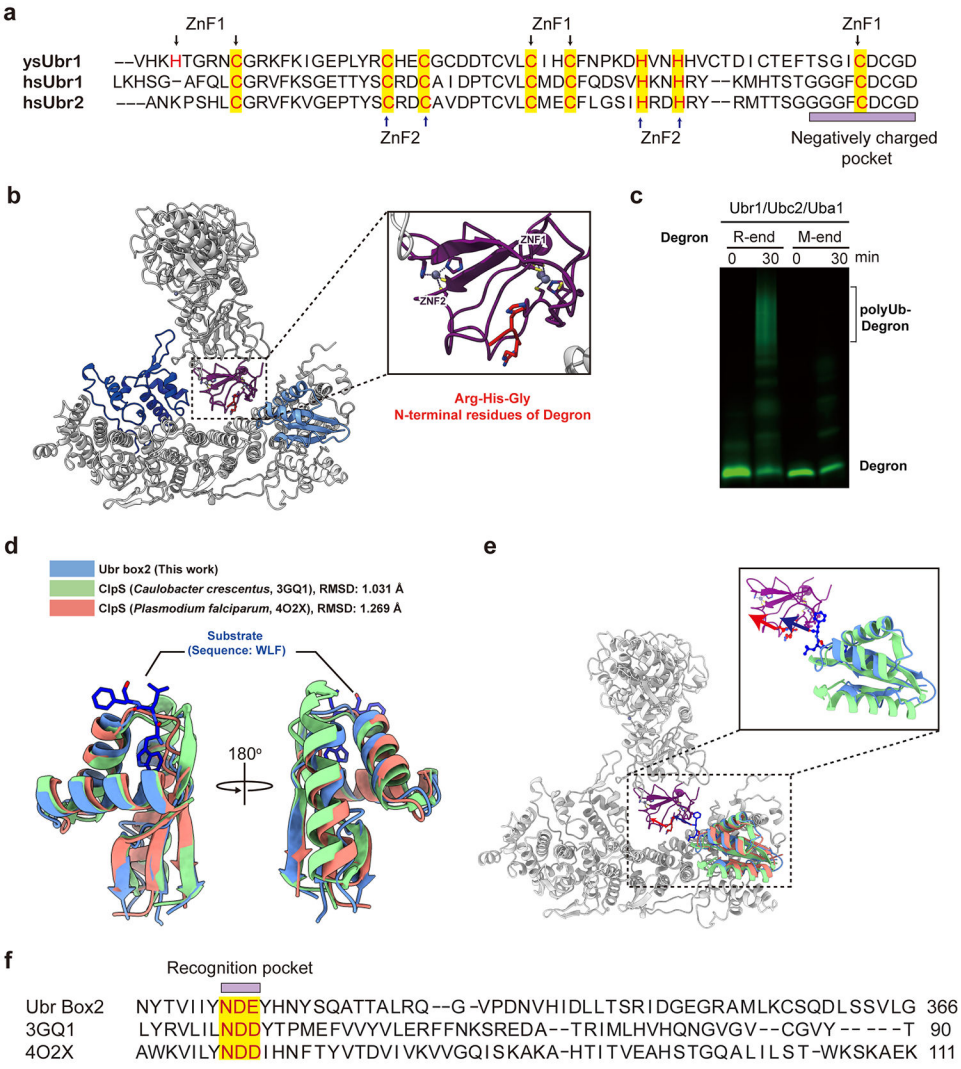

Extended Data Fig. 6: Characterization of N-degron recognition domains on Ubr1.

a, Sequence alignment of Ubr-box1 in yeast and human Ubr1 and human Ubr2. The negatively charged pocket involved in the recognition of the Arg/N-end is highlighted in light purple. **b,** A close-up view of substrate-engaged Ubr-box1. **c,** *In vitro* Ubr1-dependent ubiquitination assay on fluorescently labelled Arg/N-end degron (Degron) and Met/N-end degron (Degron with the first amino acid changed to methionine). Gel images are representative of independent biological replicates (n = 2). **d,** Structure alignment of yeast Ubr-box2 determined in this study with substrate loaded ClpS (*Caulobacter crescentus*, 3GQ1) and substrate free ClpS (*Plasmodium falciparum*, 4O2X). Root-mean-square deviation (RMSD) of backbone atoms are indicated. Substrate peptide from ClpS (*Caulobacter crescentus*, 3GQ1) is coloured in dark blue. **e,** Structure alignment of Ubr-box2 determined in this study with substrate loaded ClpS (*Caulobacter crescentus*, 3GQ1) in the context of Ubr1. The C-terminus of type-1 (this study) and type-2 (from 3GQ1) substrates

are highlighted using red and blue arrows, respectively, pointing to the active site of Ubr1. **f,** Sequence alignment of yeast Ubr-box2 with ClpS from *Caulobacter crescentus* (3GQ1) and *Plasmodium falciparum* (4O2X). The substrate binding pocket is highlighted in yellow.

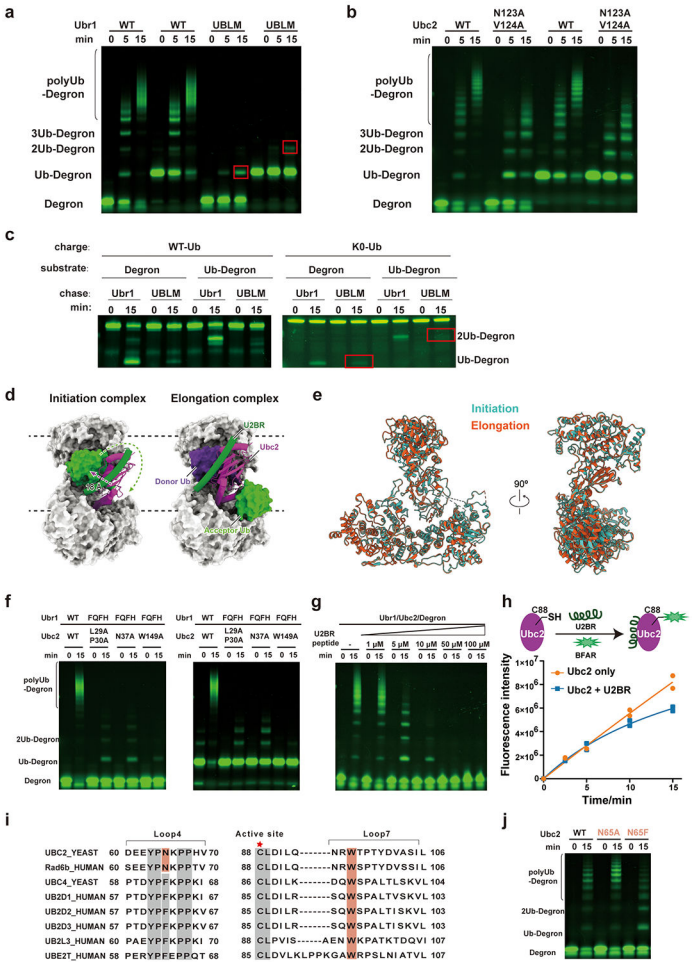

Extended Data Fig. 7: Characterization of the interfaces between Ubr1, Ubc2 and Ub.

a-b, *In vitro* Ubr1-dependent ubiquitination assays. Mutations of the Ub binding loop on Ubr1 (H678A/V679A/L680A/H681A, UBLM, panel **a**) and Ubc2 (N123A/V124A, panel **b**) were tested. Gel images are representative of independent biological replicates (n = 2). Red boxes highlight the difference of UBLM mutant in initiation and elongation. **c**, Single-turnover ubiquitination assay of wild-type Ubr1 and UBLM mutant using Ubc2 charged with either wild-type Ub or K0-Ub (all Lysine residues mutated to Arginine). Red boxes highlight the defect of UBLM mutant in elongation. Gel images are representative of independent biological replicates (n = 2). **d**, Side views of the initiation and elongation complexes showing the displacement of U2BR, Ubc2, and Ub. **e**, Alignment of Ubr1 structure in the initiation and elongation complexes. **f-g**, *In vitro* Ubr1-dependent ubiquitination assays. Gel images are representative of independent biological replicates (n = 2). **f,** Ubr1 (F1190A, Q1186A, F1183A, H1175A, FQFH mutant) and Ubc2 mutants at the interface shown in Fig. 3b were tested. **g**, The inhibition of Ubr1-dependent ubiquitination in

the presence of increasing concentrations of a synthetic U2BR peptide. **h**, The accessibility of the catalytic cysteine (Cys88) of Ubc2 was tested using fluorescein-5-maleimide, a bulky fluorescent alkylation reagent (BFAR), in the presence or absence of the synthetic U2BR peptide. The average fluorescence from two independent biological replicates was plotted ($n = 2$). **i**, Sequence alignment of multiple E2 enzymes, including yeast and human Ubc2 (also known as Rad6b in human). Two regions involved in the interaction with the RING finger domain are shown. **j**, *In vitro* Ubr1-dependent ubiquitination assays were performed to examine the role of N65 of Ubc2 in the interaction with the RING finger domain of Ubr1. Gel images are representative of independent biological replicates ($n = 2$).

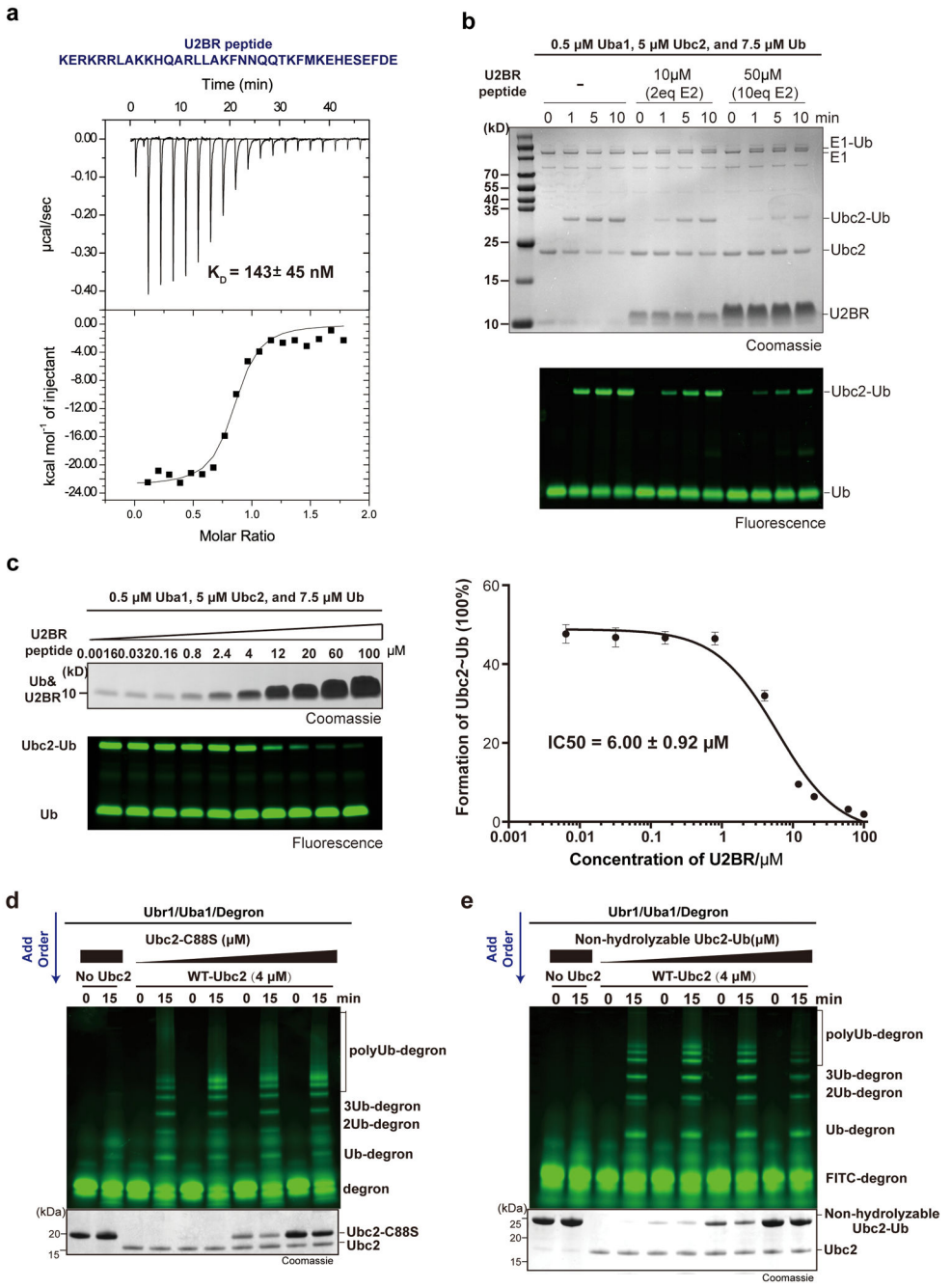

Extended Data Fig. 8: Characterization of the interactions between U2BR and Ubc2.

a, ITC measurement of the binding between Ubc2 and the synthetic U2BR peptide. **b**, The formation of E1-dependent Ubc2~Ub thioester in the presence of the synthetic U2BR peptide. Gel images are representative of independent biological replicates (n = 2). **c**, Quantitative evaluation of the inhibitory effect of the synthetic U2BR peptide on E1-dependent Ubc2~Ub thioester formation. Averages of three independent biological replicates (n = 3) were plotted and fit to estimate the IC50 of the synthetic U2BR peptide. The curves are presented as mean values ± s.d.. **d-e**, *In vitro* Ubr1-dependent ubiquitination assay. Increasing doses of catalytically inactive Ubc2-C88S (**b**) and non-hydrolysable Ubc2-Ub (**c**)

up to 12.5 μM were pre-mixed with Ubr1, followed by adding wild-type Ubc2 at 4 μM. Gel images are representative of independent biological replicates (n = 2).

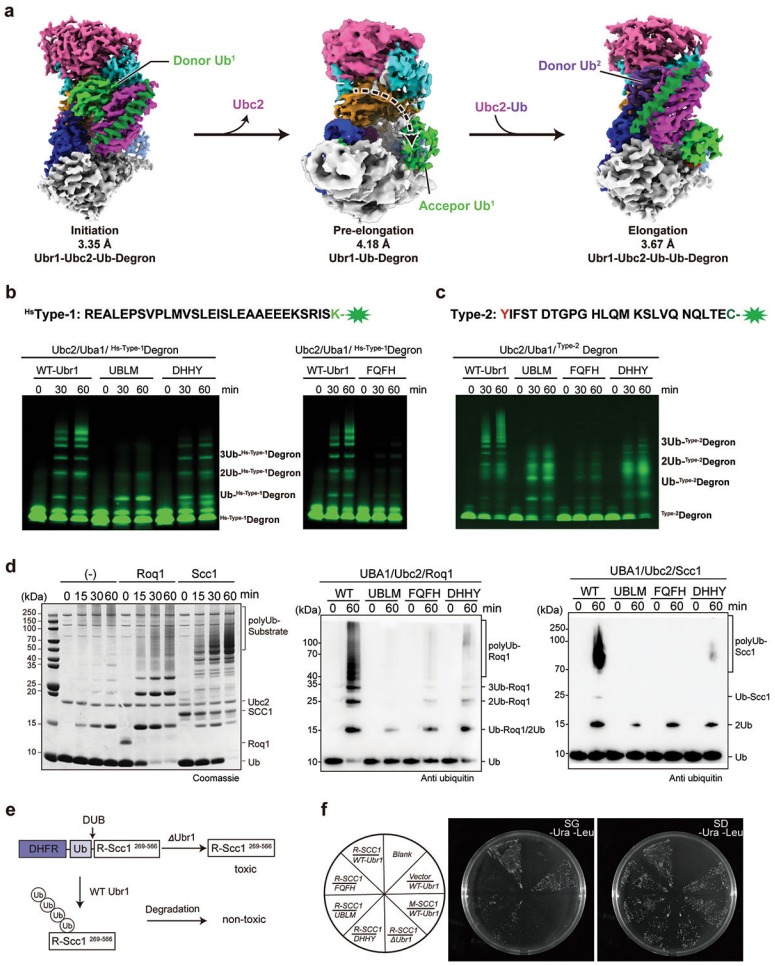

Extended Data Fig. 9: Structure of pre-elongation complex and validation of structural mechanism.

a, Comparison of initiation, pre-elongation and elongation complex in the same orientation showing the movement of donor ubiquitin. The colour code of Ubr1 is the same as that in Fig. 1b. Sharpened map of the pre-elongation complex is shown at a contour level of 0.011. **b**, *In vitro* ubiquitination assay on fluorescently labelled ^{Hs}-Type-1 Degron (derived from human protein Rec8) with wild-type Ubr1 and Ubr1 mutants, UBLM, DHHY and FQFH. Gel images are representative of independent biological replicates (n = 2). **c**, *In vitro* ubiquitination assay on fluorescently labelled Type-2 Degron (derived from Sindbis virus polymerase nsP4) with wild-type Ubr1 and Ubr1 mutants, UBLM, DHHY and FQFH. Gel images are representative of independent biological replicates (n = 2). **d**, *In vitro* ubiquitination assay on truncated protein substrates ROQ1 (22-104) and Scc1 (268-384) with wild-type Ubr1 and Ubr1 mutants, UBLM, DHHY and FQFH. Gel images are representative of independent biological replicates (n = 2). **e,** Design of the yeast-growth assay. Endogenous deubiquitinating enzymes (DUB) cleave the construct co-translationally and produce Scc1 fragment (R-Scc1$^{269\text{-}566}$) which has an N-terminal arginine residue and

is toxic to the yeast strain deficient of Ubr1 (ΔUbr1). If wild-type Ubr1 is supplemented, R-Scc1$^{269\text{-}566}$ will be rapidly polyubiquitinated and degraded, reversing the growth defect. **f.** Yeast strains carrying wild-type Ubr1 or Ubr1 mutants (FQFH, UBLM and DHHY) were streaked either on dextrose-containing (SD) plates (right) where all strains grew without the expression of Scc1 fragment and Ubr1 variants, or on galactose containing (SG) plates (left), where all strains grew with the induced gene expression of Scc1 fragment and Ubr1 variants. In addition to R-Scc1$^{269\text{-}566}$, M-Scc1$^{269\text{-}566}$ which has an N-terminal methionine residue was also tested. The plates were incubated at 30 °C for 3 days.

Extended Data Table 1:

Cryo-EM data collection, refinement and validation statistics.

	Initiation complex (EMDB-23806) (PDB 7MEX)	**Elongation complex (EMDB-23807) (PDB 7MEY)**	**Pre-elongation complex (EMDB-24935)**	**Apo-Ubr1 (EMDB-24936)**
Data collection and processing				
Magnification	81,000	81,000	81,000	81,000
Voltage (kV)	300	300	300	300
Electron exposure (e–/Å^2)	50	50	50	50
Defocus range (μm)	−1.0 to −2.5	−1.0 to −2.5	−1.0 to −2.5	−1.0 to −2.5
Pixel size (Å)	1.063	1.063	1.065	1.122
Symmetry imposed	C1	C1	C1	C1
Initial particle images (no.)	1,643,874	646,482	1,765,032	636,808
Final particle images (no.)	232,915	65,088	193,669	30,415
Map resolution (Å)	3.35	3.67	4.18	4.56
FSC threshold	0.143	0.143	0.143	0.143
Refinement				
Model resolution (Å)	3.46	3.83		
FSC threshold	0.5	0.5		
Map sharpening *B* factor (Å^2)	−96.5	−96.7		
Model composition				
Non-hydrogen atoms	15941	16468		
Protein residues	1967	2033		
Ligands	Zn: 7	Zn: 7 ETE: 1 (chemical linker)		
B factors (Å^2)				
Protein	43.78	87.17		
Ligand	70.81	122.04		
R.m.s. deviations				
Bond lengths (Å)	0.003	0.003		
Bond angles (°)	0.519	0.541		
Validation				
MolProbity score	1.48	1.75		
Clashscore	8.11	10.74		
Poor rotamers (%)	0.06	0.00		

	Initiation complex (EMDB-23806) (PDB 7MEX)	Elongation complex (EMDB-23807) (PDB 7MEY)	Pre-elongation complex (EMDB-24935)	Apo-Ubr1 (EMDB-24936)
Ramachandran plot				
Favored (%)	97.84	96.77		
Allowed (%)	2.16	3.23		
Disallowed (%)	0.00	0.00		

Supplementary Material

Refer to Web version on PubMed Central for supplementary material.

Acknowledgements

We thank the staff at the National Cryo-Electron Microscopy Facility at the Frederick National Laboratory and the Advanced Electron Microscopy Facility at the University of Chicago for the help in cryo-EM data collection. We thank Dr. Hai Rao (Southern University of Science and Technology) and Dr. Ronggui Hu (University of Chinese Academy of Sciences) for their kind help in yeast related experiments. Funding: Funding for this work was, in part, provided by the Catalyst Award from the Chicago Biomedical Consortium. This work was supported by Chicago Biomedical Consortium Catalyst Award C-086 to M.Z. We thank t the National Key R&D Program of China (no. 2017YFA0505200) and NSFC (91753205, 81621002, 21621003) for financial support., National Postdoctoral Program for Innovative Talents (BX2021143), Shuimu Tsinghua Scholar Program (2021SM067) for financial support. This research was, in part, supported by the National Cancer Institute's National Cryo-EM Facility at the Frederick National Laboratory for Cancer Research under contract HSSN261200800001E. This material is based upon work supported by the National Science Foundation under Grant No. 2030381, the graduate research award of Computing and Software Systems division, and the start-up fund 74–0525 at University of Washington Bothell to D.S·· Any opinions, findings, and conclusions or recommendations expressed in this material are those of the authors and do not necessarily reflect the views of the National Science Foundation. Molecular graphics and analyses were performed with UCSF ChimeraX, developed by the Resource for Biocomputing, Visualization, and Informatics at the University of California, San Francisco, with support from National Institutes of Health R01-GM129325 and the Office of Cyber Infrastructure and Computational Biology, National Institute of Allergy and Infectious Diseases.

Data availability

Cryo-EM maps have been deposited in the Electron Microscopy Data Bank (EMDB, www.ebi.ac.uk/pdbe/emdb/) under the accession codes EMDB-23806 (initiation complex), EMDB-23807 (elongation complex), EMDB-24935 (pre-elongation complex), and EMDB-24936 (apo-Ubr1). The atomic models have been deposited in the Protein Data Bank (PDB, www.rcsb.org) under the accession codes 7MEX (initiation complex) and 7MEY (elongation complex). The atomic model of UbcH5 and the RING finger domain of TRIM25 is available under the PDB accession code 5FER. Uncropped gels and blots source data have been included as Supplementary Information Fig. 7. Due to the large file size, raw electron microscopy data are available from the corresponding authors upon request.

REFERENCES

1. Chau V, Tobias JW, Bachmair A, Marriott D, Ecker DJ, Gonda DK, & Varshavsky A A Multiubiquitin Chain Is Confined to Specific Lysine in a Targeted Short-Lived Protein. Science 243, 1576–1583 (1989). [PubMed: 2538923]
2. Bartel B, Wunning I & Varshavsky A The recognition component of the N-end rule pathway. EMBO. J 9, 3179–3189 (1990). [PubMed: 2209542]

3. Komander D & Rape M The Ubiquitin Code. Annu. Rev. Biochem 81, 203–229 (2012). [PubMed: 22524316]
4. Chen SJ, Wu X, Wadas B, Oh JH & Varshavsky A An N-end rule pathway that recognizes proline and destroys gluconeogenic enzymes. Science 355, 6323 (2017).
5. Kim JM, Seok OH, Ju S, Heo JE, Yeom J, Kim DS, Yoo JY, Varshavsky A, Lee C & Hwang CS Formyl-methionine as an N-degron of a eukaryotic N-end rule pathway. Science 362, eaat0174. (2018). [PubMed: 30409808]
6. Tasaki T, Sriram SM, Park KS & Kwon YT The N-end rule pathway. Annu. Rev. Biochem 81, 261–289 (2012). [PubMed: 22524314]
7. Varshavsky A The N-end rule pathway and regulation by proteolysis. Protein Sci. 20, 1298–1345 (2011). [PubMed: 21633985]
8. Zenker M, Mayerle J, Lerch MM, Tagariello A, Zerres K, Durie PR, … & Reis A Deficiency of UBR1, a ubiquitin ligase of the N-end rule pathway, causes pancreatic dysfunction, malformations and mental retardation (Johanson-Blizzard syndrome). Nat. Genet 37, 1345–1350 (2005). [PubMed: 16311597]
9. Bodnar NO & Rapoport TA Molecular Mechanism of Substrate Processing by the Cdc48 ATPase Complex. Cell 169, 722–735 (2017). [PubMed: 28475898]
10. Petroski MD & Deshaies RJ Mechanism of lysine 48-linked ubiquitin-chain synthesis by the cullin-RING ubiquitin-ligase complex SCF-Cdc34. Cell 123, 1107–1120 (2005). [PubMed: 16360039]
11. Saha A & Deshaies RJ Multimodal Activation of the Ubiquitin Ligase SCF by Nedd8 Conjugation. Mol. Cell 32, 21–31 (2008). [PubMed: 18851830]
12. Tasaki T, Zakrzewska A, Dudgeon DD, Jiang Y, Lazo JS, & Kwon YT The substrate recognition domains of the N-end rule pathway. J. Biol. Chem 284, 1884–1895 (2009). [PubMed: 19008229]
13. Baek K, Krist DT, Prabu JR, Hill S, Klügel M, Neumaier LM, … & Schulman BA NEDD8 nucleates a multivalent cullin-RING-UBE2D ubiquitin ligation assembly. Nature 578, 461–466 (2020). [PubMed: 32051583]
14. Horn-Ghetko D, Krist DT, Prabu JR, Baek K, Mulder MP, Klügel M, … & Schulman BA Ubiquitin ligation to F-box protein targets by SCF-RBR E3-E3 super-assembly. Nature 590, 671–676 (2021). [PubMed: 33536622]
15. Rusnac DV & Zheng N Structural Biology of CRL Ubiquitin Ligases. Adv. Exp. Med. Biol 1217, 9–31 (2020). [PubMed: 31898219]
16. Matta-Camacho E, Kozlov G, Li FF & Gehring K Structural basis of substrate recognition and specificity in the N-end rule pathway. Nat. Struct. Mol. Biol 17, 1182–1187 (2010). [PubMed: 20835242]
17. Choi WS et al. Structural basis for the recognition of N-end rule substrates by the UBR box of ubiquitin ligases. Nat. Struct. Mol. Biol 17, 1175–1181 (2010). [PubMed: 20835240]
18. Du FY, Navarro-Garcia F, Xia ZX, Tasaki T & Varshavsky A Pairs of dipeptides synergistically activate the binding of substrate by ubiquitin ligase through dissociation of its autoinhibitory domain. Proc. Natl. Acad. Sci. USA 99, 14110–14115 (2002). [PubMed: 12391316]
19. Roman-Hernandez G, Grant RA, Sauer RT & Baker TA Molecular basis of substrate selection by the N-end rule adaptor protein ClpS. Proc. Natl. Acad. Sci. U S A 106, 8888–93 (2009). [PubMed: 19451643]
20. AhYoung AP, Koehl A, Vizcarra CL, Cascio D & Egea PF Structure of a putative ClpS N-end rule adaptor protein from the malaria pathogen Plasmodium falciparum. Protein Sci. 25, 689–701 (2016). [PubMed: 26701219]
21. Kim L et al. Structural basis for the N-degron specificity of ClpS1 from Arabidopsis thaliana. Protein Sci. 30, 700–708 (2021). [PubMed: 33368743]
22. Das R, Mariano J, Tsai YC, Kalathur RC, Kostova Z, Li J, … & Weissman AM Allosteric activation of E2-RING finger-mediated ubiquitylation by a structurally defined specific E2-binding region of gp78. Mol. Cell 34, 674–685 (2009). [PubMed: 19560420]
23. Metzger MB, Liang YH, Das R, Mariano J, Li S, Li J, … & Weissman AM A Structurally Unique E2-Binding Domain Activates Ubiquitination by the ERAD E2, Ubc7p, through Multiple Mechanisms. Mol. Cell 50, 516–527 (2013). [PubMed: 23665230]

24. Koliopoulos MG, Esposito D, Christodoulou E, Taylor IA & Rittinger K Functional role of TRIM E3 ligase oligomerization and regulation of catalytic activity. Embo J. 35, 1204–1218 (2016). [PubMed: 27154206]
25. Plechanovova A, Jaffray EG, Tatham MH, Naismith JH & Hay RT Structure of a RING E3 ligase and ubiquitin-loaded E2 primed for catalysis. Nature 489, 115–120 (2012). [PubMed: 22842904]
26. Zheng Q, Wang T, Chu GC, Zuo C, Zhao R, Sui X, … & Liu L An E1-Catalyzed Chemoenzymatic Strategy to Isopeptide-N-Ethylated Deubiquitylase-Resistant Ubiquitin Probes. Angew. Chem. Int. Ed. Engl 59, 13496–13501 (2020). [PubMed: 32346954]
27. Liu YJ et al. Degradation of the Separase-cleaved Rec8, a Meiotic Cohesin Subunit, by the N-end Rule Pathway. J. Biol. Chem 291, 7426–7438 (2016). [PubMed: 26858254]
28. Degroot RJ, Rumenapf T, Kuhn RJ, Strauss EG & Strauss JH Sindbis Virus-Rna Polymerase Is Degraded by the N-End Rule Pathway. Proc. Natl. Acad. Sci. USA 88, 8967–8971 (1991). [PubMed: 1924357]
29. Rao H, Uhlmann F, Nasmyth K & Varshavsky A Degradation of a cohesin subunit by the N-end rule pathway is essential for chromosome stability. Nature 410, 955–959 (2001). [PubMed: 11309624]
30. Szoradi T et al. SHRED Is a Regulatory Cascade that Reprograms Ubr1 Substrate Specificity for Enhanced Protein Quality Control during Stress. Mol. Cell 70, 1025–1037 (2018). [PubMed: 29861160]
31. Streich FC Jr. & Lima CD Capturing a substrate in an activated RING E3/E2-SUMO complex. Nature 536, 304–308 (2016). [PubMed: 27509863]
32. Xia Z, Webster A, Du F, Piatkov K, Ghislain M, & Varshavsky A Substrate-binding sites of UBR1, the ubiquitin ligase of the N-end rule pathway. J. Biol. Chem 283, 24011–24028 (2008). [PubMed: 18566452]
33. Pan M, Zheng Q, Ding S, Zhang L, Qu Q, Wang T, … & Liu L Chemical Protein Synthesis Enabled Mechanistic Studies on the Molecular Recognition of K27-linked Ubiquitin Chains. Angew. Chem. Int. Ed. Engl 58, 2627–2631 (2019). [PubMed: 30589182]
34. Pan M, Gao S, Zheng Y, Tan X, Lan H, Tan X, Sun D, Lu L, Wang T, Zheng Q and Huang Y, Wang J & Liu L Quasi-Racemic X-ray Structures of K27-Linked Ubiquitin Chains Prepared by Total Chemical Synthesis. J. Am. Chem. Soc 138, 7429–7435 (2016). [PubMed: 27268299]
35. Qu Q, Pan M, Gao S, Zheng QY, Yu YY, Su JC, … & Hu HG A Highly Efficient Synthesis of Polyubiquitin Chains. Adv Sci (Weinh) 5, 1800234 (2018). [PubMed: 30027052]
36. Zheng SQ, Palovcak E, Armache JP, Verba KA, Cheng Y, & Agard DA MotionCor2: anisotropic correction of beam-induced motion for improved cryo-electron microscopy. Nat. Methods 14, 331–332 (2017). [PubMed: 28250466]
37. Mindell JA & Grigorieff N Accurate determination of local defocus and specimen tilt in electron microscopy. J. Struct. Biol 142, 334–47 (2003). [PubMed: 12781660]
38. Zivanov J, Nakane T, Forsberg BO, Kimanius D, Hagen WJ, Lindahl E, & Scheres SH New tools for automated high-resolution cryo-EM structure determination in RELION-3. Elife 7, e42166 (2018). [PubMed: 30412051]
39. Pfab J, Phan NM & Si D DeepTracer for fast de novo cryo-EM protein structure modeling and special studies on CoV-related complexes. Proc. Natl. Acad. Sci. USA 118, e2017525118 (2021). [PubMed: 33361332]
40. Adams PD, Afonine PV, Bunkóczi G, Chen VB, Davis IW, Echols N, … & Zwart PH PHENIX: a comprehensive Python-based system for macromolecular structure solution. Acta. Crystallogr. D. Biol. Crystallogr 66, 213–221 (2010). [PubMed: 20124702]
41. Emsley P & Cowtan K Coot: model-building tools for molecular graphics. Acta. Crystallogr. D. Biol. Crystallogr 60, 2126–32 (2004). [PubMed: 15572765]
42. Croll TI ISOLDE: a physically realistic environment for model building into low-resolution electron-density maps. Acta Crystallogr D Struct Biol 74, 519–530 (2018). [PubMed: 29872003]
43. Pettersen EF et al. UCSF ChimeraX: Structure visualization for researchers, educators, and developers. Protein Sci. 30, 70–82 (2021). [PubMed: 32881101]
44. Krissinel E & Henrick K Inference of macromolecular assemblies from crystalline state. J. Mol. Biol 372, 774–797 (2007). [PubMed: 17681537]

45. Holm L DALI and the persistence of protein shape. Protein Sci. 29, 128–140 (2020). [PubMed: 31606894]

46. Waterhouse A Bertoni M, Bienert S, Studer G, Tauriello G, Gumienny R, … & Schwede T SWISS-MODEL: homology modelling of protein structures and complexes. Nucleic. Acids. Res. 46, W296–W303 (2018). [PubMed: 29788355]

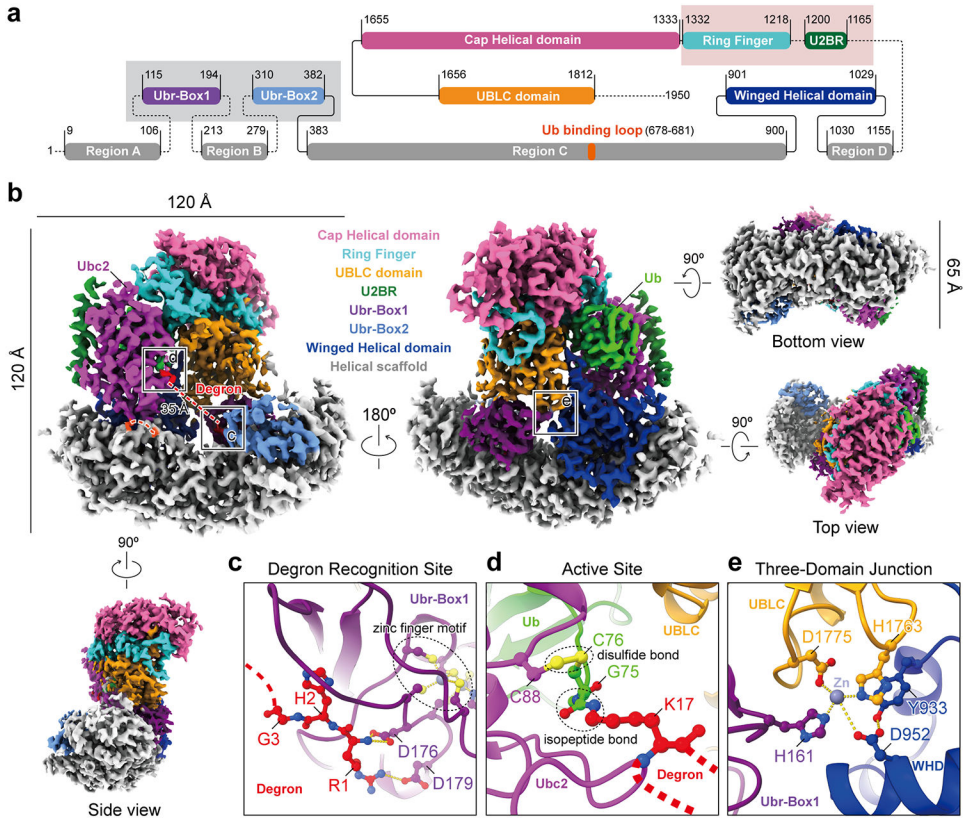

FIG. 1: Structure of the initiation complex.

a, A schematic domain diagram of Ubr1, with residue boundaries indicated. Dotted lines represent unresolved linkers and regions. Grey box: Substrate recruiting domains; Pink box: Ubc2 recruiting domains. **b**, Cryo-EM maps of the initiation complex (sharpened using a B factor of −96.5 Å^2, contour level: 0.030). The colour code of Ubr1 is the same as that in panel **a. c,** Molecular interactions between Degron and Ubr-Box1. Hydrogen bonds and electrostatic interactions are represented by dotted lines. **d,** Molecular structure of the active site. **e,** Molecular interactions between UBLC, Ubr-Box1 and the winged helical domain (WHD). Metal coordination bonds and hydrogen bonds are represented by dotted lines.

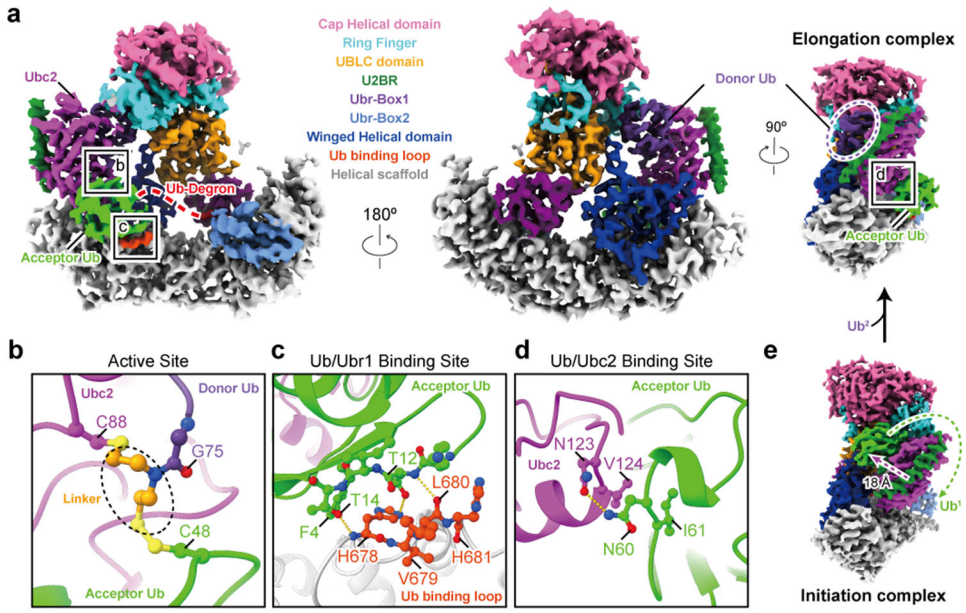

FIG. 2: Structure of the elongation complex.

a, Cryo-EM maps of the elongation complex (sharpened using a B factor of −96.7 Å^2, contour level: 0.022). The colour code of Ubr1 is the same as that in Fig. 1a. **b,** Molecular structure of the active site. **c,** Molecular interactions between acceptor Ub and the Ub binding loop of Ubr1. Hydrogen bonds are represented by dotted lines. **d**, Molecular interactions between acceptor Ub and Ubc2. Hydrogen bonds are represented by dotted lines. **e**, A side view of the initiation complex in the same orientation as that of the elongation complex in panel **a**. Displacement of Ubc2, U2BR, and Ub are noted with arrows.

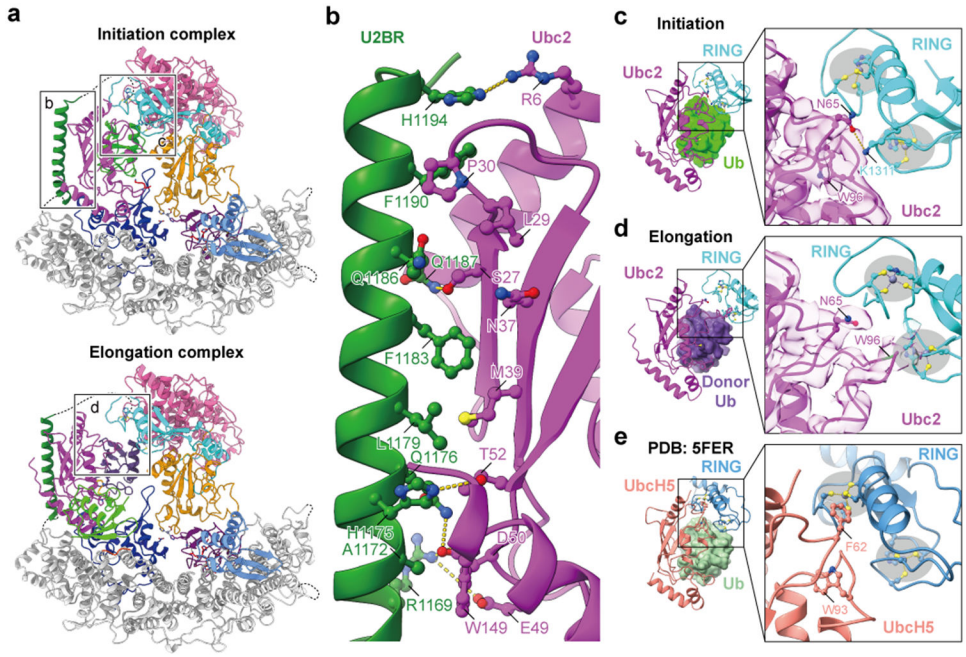

FIG. 3: Analyses of the interactions between Ubc2 and Ubr1.

a, Molecular structures of the initiation complex and the elongation complex. **b**, A close-up view of the interface between Ubc2 and U2BR of Ubr1. Labelled residues are involved in extensive noncovalent interactions. Hydrogen bonds and electrostatic interactions are represented by dotted lines. **c-e**, Close-up views of the interface between E2 and RING finger domains. **c**, Ubc2 and the RING finger domain in the initiation complex. Hydrogen bonds are represented by dotted lines. Density of Ubc2 is from the same map in Fig. 1b contoured at 0.030. **d,** Ubc2 and the RING finger domain in the elongation complex. Note that due to the flexibility, the side chains of the loop around W96 (marked green) could not be accurately built into the density. Density of Ubc2 is from the same map in Fig. 2a contoured at 0.020. **e,** UbcH5 and the RING finger domain of TRIM25 (PDB: 5FER) [25].

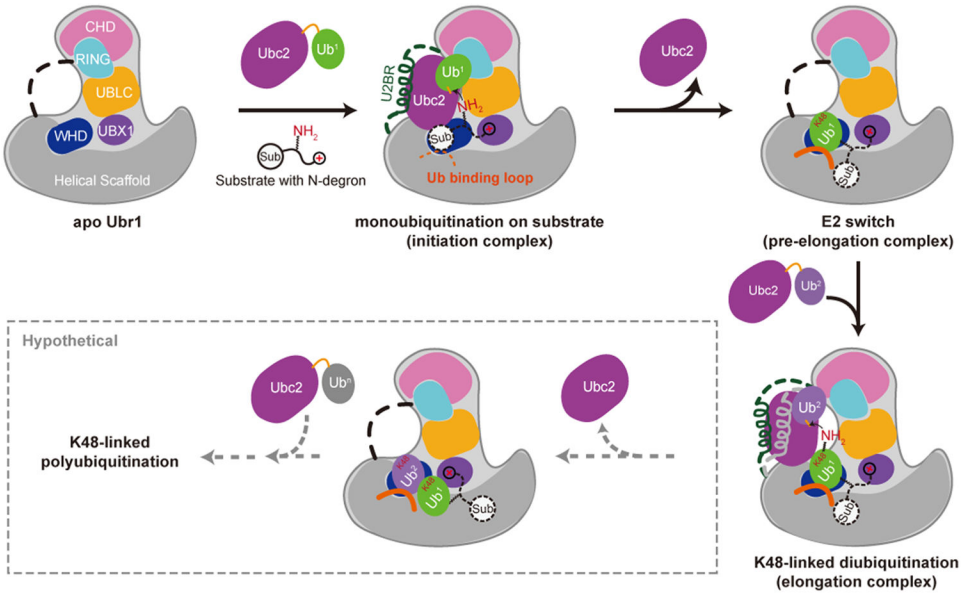

FIG. 4: A model of Ubr1-mediated polyubiquitination.

A cartoon representation of Ubr1-mediated polyubiquitination starting from a degron peptide with a positively charged N-terminal residue (type-1 degron). The first three steps correspond to the initiation, pre-elongation and elongation structures described in this study. Subsequent elongation of the polyubiquitin chain is hypothetical. The Ub molecules being conjugated are sequentially numbered as Ub^1, Ub^2, Ub^n.